

APPENDICES

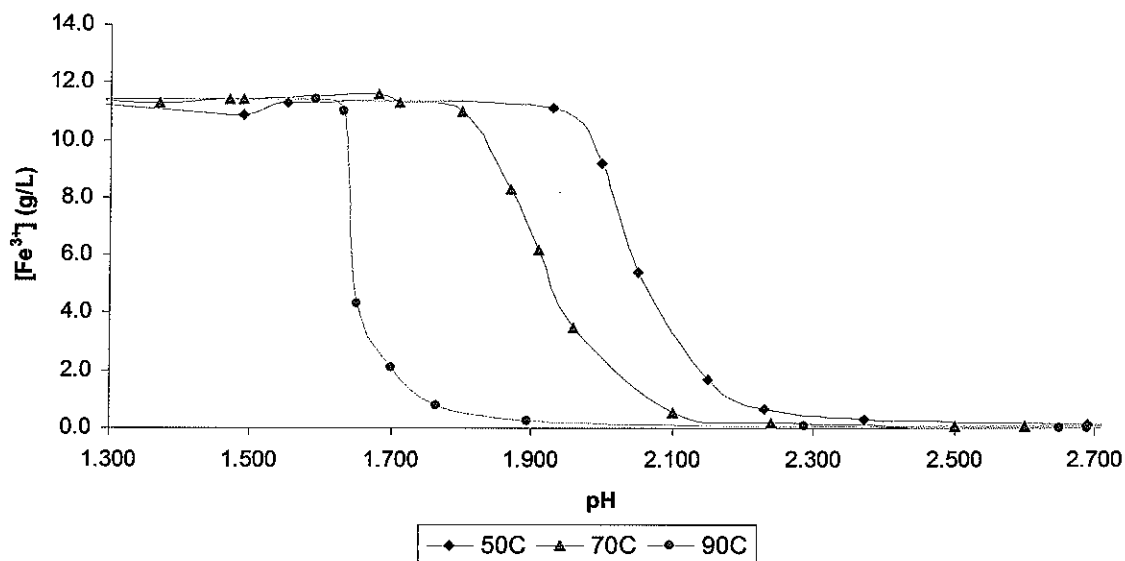
Appendix 1: Ferric iron nucleation and solubility curves

Figure A1.1. Nucleation data for ferric iron determined at 50, 70 and 90°C. The pH was changed stepwise in increments of 0.5 pH units every 20 minutes. The pH was controlled by adding $\text{Ca}(\text{OH})_2$, ZnO powder and 98% H_2SO_4 .

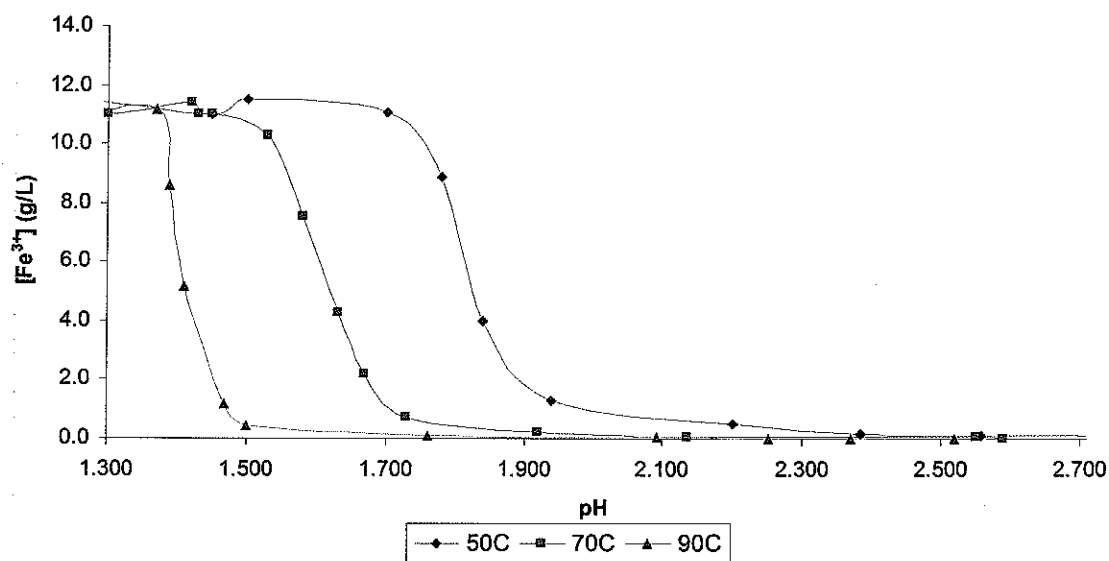


Figure A1.2. Solubilization data for ferric iron determined at 50, 70 and 90°C. The pH was changed stepwise in increments of 0.5 pH units every 20 minutes. The pH was controlled by adding $\text{Ca}(\text{OH})_2$, ZnO powder and 98% H_2SO_4 .

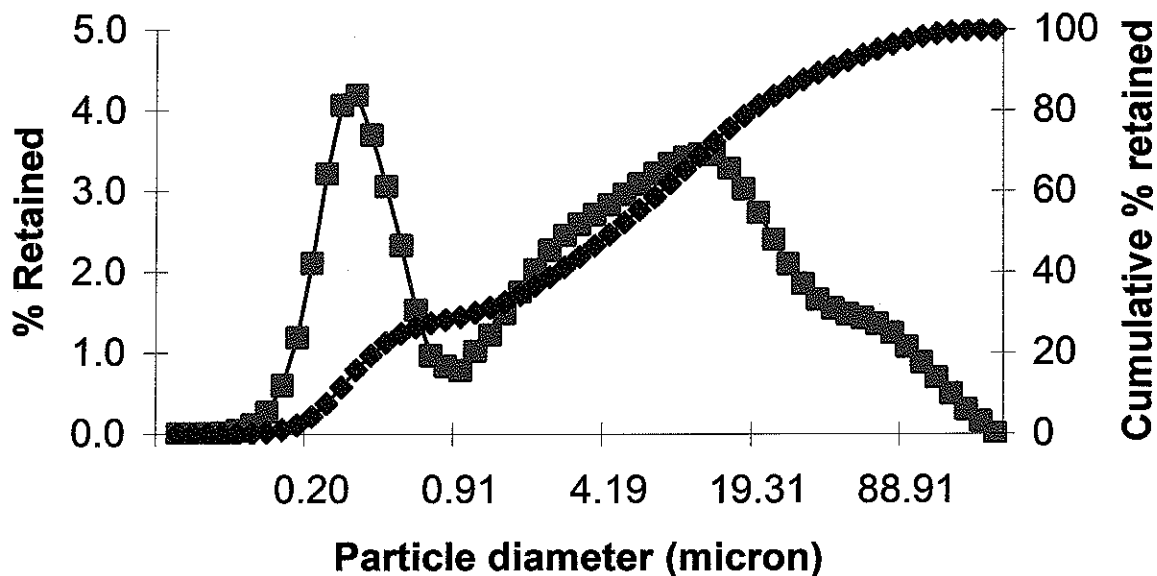


Figure A1.3. Particle size distribution of the seed material used to determine the influence of seed mass on agglomeration as determined by a Malvern Mastersizer.

Appendix 2: Ferric iron equilibrium solubility data as calculated by STABCAL™

Ferric stability at 50C

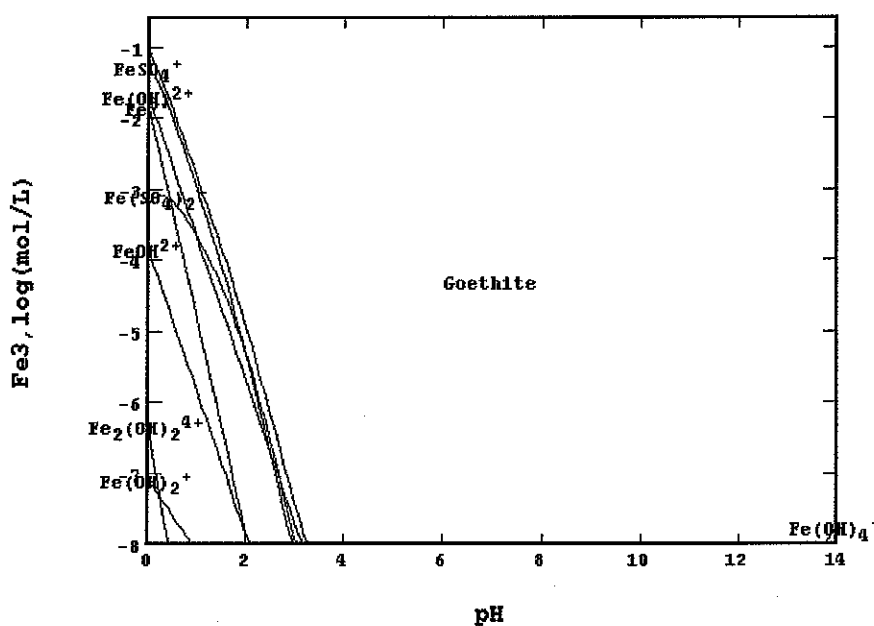


Figure A2.1. Ferric ion stability diagram determined with the STABCAL™ NBS-database at 50°C.

Ferric stability at 70C

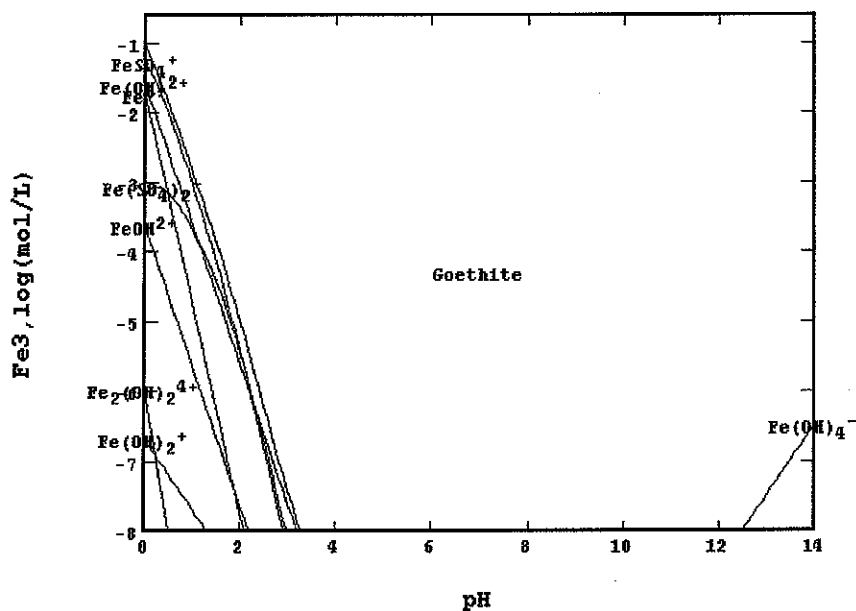


Figure A2.2. Ferric ion stability diagram determined with the STABCAL™ NBS-database at 70°C.

Ferric stability at 90C

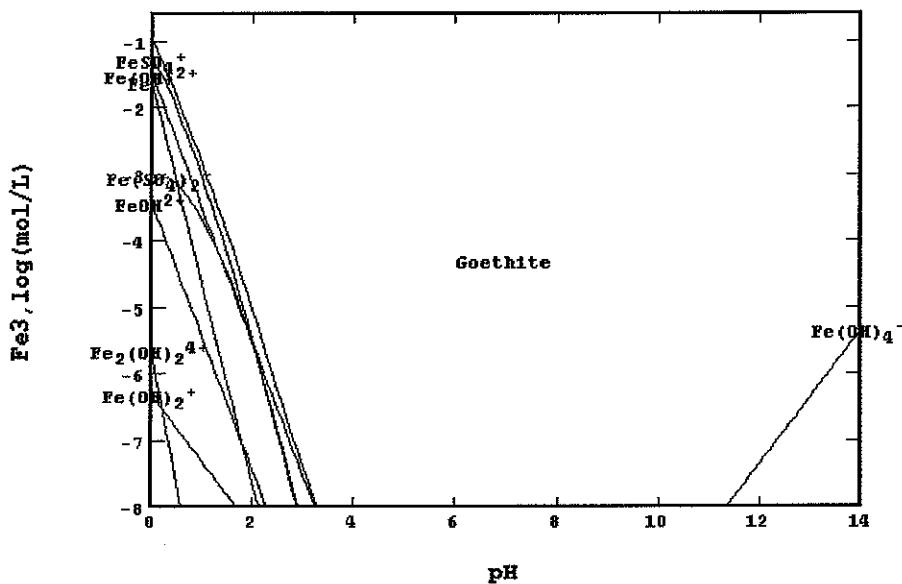


Figure A2.3. Ferric ion stability diagram determined with the STABCAL™ NBS-database at 90°C.

Appendix 3:

Table A3.1. Spreadsheet used to calculate particle population density from Malvern particle analysis data.

total solid mass (g)	5.00E+01	measured from the total mass of sample or calculated from a process mass balance				
rho solid (kg/m3)	3232					
vol ppted (m3)	1.55E-05					
*SIZES*um	Vol %	Delta L (m)	Lbar (m)	N (1/m3)	n(L) (1/m4) =N/Delta L	n(L) * Lbar (1/m3)
0.05	0.00					
0.06	0.00041	1.00E-08	6.50E-08	2.83E+12	2.83E+20	1.84E+13
0.07	0.00126	1.00E-08	7.50E-08	2.87E+11	2.87E+19	2.15E+12
0.08	0.00326	1.00E-08	8.50E-08	6.06E+11	6.06E+19	5.15E+12
0.09	0.00836	1.00E-08	9.50E-08	1.12E+12	1.12E+20	1.07E+13
0.11	0.02145	2.00E-08	1.20E-07	1.43E+12	7.15E+19	8.58E+12
0.13	0.05364	1.50E-08	1.33E-07	2.72E+12	1.82E+20	2.41E+13
0.15	0.12592	2.06E-08	1.56E-07	4.18E+12	2.03E+20	3.17E+13
41.43	0.56831	5.87E-06	4.44E-05	2.42E+06	4.13E+11	1.83E+07
48.27	0.39668	6.84E-06	5.17E-05	1.22E+06	1.78E+11	9.20E+06
56.23	0.21086	7.96E-06	6.02E-05	5.37E+05	6.74E+10	4.06E+06
65.51	0.05121	9.28E-06	7.01E-05	1.81E+05	1.95E+10	1.36E+06
76.32	0.00937	1.08E-05	8.17E-05	2.77E+04	2.57E+09	2.10E+05
88.91	0.00258	1.26E-05	9.52E-05	3.21E+03	2.55E+08	2.43E+04
103.58	0.00051	1.47E-05	1.11E-04	5.59E+02	3.81E+07	4.22E+03
120.67	0.00007	1.71E-05	1.29E-04	6.98E+01	4.09E+06	5.28E+02
140.58	0	1.99E-05	1.51E-04	6.06E+00	3.05E+05	4.58E+01
163.77	0.00764	2.32E-05	1.75E-04	0.00E+00	0.00E+00	0.00E+00
190.80	0.50994	2.70E-05	2.04E-04	2.65E+02	9.80E+06	2.00E+03
222.28	1.92305	3.15E-05	2.38E-04	1.12E+04	3.55E+08	8.45E+04
258.95	3.96071	3.67E-05	2.77E-04	2.66E+04	7.27E+08	2.01E+05
301.68	4.71965	4.27E-05	3.23E-04	3.47E+04	8.12E+08	2.62E+05
351.46	3.57416	4.98E-05	3.76E-04	2.62E+04	5.26E+08	1.98E+05
409.45	1.78791	5.80E-05	4.38E-04	1.25E+04	2.16E+08	9.47E+04
477.01	0.46826	6.76E-05	5.11E-04	3.96E+03	5.87E+07	3.00E+04
555.71	0	7.87E-05	5.95E-04	6.57E+02	8.34E+06	4.96E+03
647.41	0	9.17E-05	6.93E-04	0.00E+00	0.00E+00	0.00E+00
			m0	8.19E+13		
			m1	8.89E+06		
			m2	3.77E+00		
			m3	8.98E-06		
			m4	1.34E-10		
			lbar1,0	1.09E-07		

LIST OF FIGURES

Figure 1: Decision diagram to choose the method of crystallization [After Van Rosmalen and Kramer, 1998]. C_{eq} = equilibrium solution concentration of element being removed. p.20

Figure 2. Iron removal processes used in the zinc industry to purify zinc-rich process solutions [After Claassen *et al.*, 2003(b)]. p.23

Figure 3: Simplified jarosite precipitation flowsheet [Arregui *et al.*, 1980]. p.24

Figure 4. Simplified diagram of precipitation characteristics of various inorganic salts [After Gösele *et al.* 1990]. O = crystalline product, Δ = temporary gelatinous, ● = permanent gelatinous. p.28

Figure 5. Stability diagram showing the conditions for the precipitation of different iron phases from 0.5 M ferric sulphate solutions [Babcan, 1971]. Hydroxy salts = basic iron sulphates. p.29

Figure 6. Dimensions of the crystallizer used to determine the influence of stagewise precipitation on product quality. p.32

Figure 7. Average ferric iron concentration as a function of pH determined at 50°C. The pH was changed stepwise in increments of 0.5 pH units every 20 minutes. The pH was increased by adding Ca(OH)_2 and ZnO powder and decreased by adding 98% H_2SO_4 . The total sulphate concentration varied between 0.2 and 0.25 moles/L . p.36

Figure 8. Average ferric iron concentration as a function of pH determined at 70°C. The pH was changed stepwise in increments of 0.5 pH units every 20 minutes. The pH was increased by adding Ca(OH)_2 and ZnO powder and decreased by adding 98% H_2SO_4 . p.37

Figure 9. Average ferric iron concentration as a function of pH determined at 90°C. The pH was changed stepwise in increments of 0.5 pH units every 20 minutes. The pH was increased by adding Ca(OH)₂ and ZnO powder and decreased by adding 98% H₂SO₄. p.37

Figure 10. Illustration of the metastable zone determined for the precipitation of iron from a ferric iron solution containing approximately 11.5 g/L Fe as Fe₂(SO₄)₃ and 5 g/L H₂SO₄. The pH was varied using Ca(OH)₂ - and ZnO powder and 98% H₂SO₄. p.38

Figure 11. Ferric concentration as a function of pH for the precipitation of iron at 50°C from a ferric iron solution containing approximately 11.5 g/L Fe as Fe₂(SO₄)₃ and 5 g/L H₂SO₄. The pH was varied using Ca(OH)₂ - and ZnO powder and 98% H₂SO₄. The experimental reverse cycle line forms the new solubility limit. p.39

Figure 12. Calculated relative supersaturation as a function of pH at different temperatures for the hydrolysis of ferric iron from iron solutions containing approximately 11.5 g/L Fe added as Fe₂(SO₄)₃ using Ca(OH)₂- and ZnO powder to control the pH. p.41

Figure 13. SEM backscattered image of an iron bearing particle, showing open structured ferrihydrite particles (Particles A) covered with a more dense structured schwertmannite layer (Portion B) [Claassen *et al.*, 2002]. p.42

Figure 14. Metastability diagram for ferric iron hydrolysis from a 10 g/L Fe (as Fe₂SO₄)₃ solution using ZnO powder to control the pH. ● = 6-line ferrihydrite and schwertmannite and ▲ = 2-line ferrihydrite obtained from XRD analyses. p.43

Figure 15. Influence of pH and temperature on the sulphate content of iron precipitated from a hot iron solution containing 10 g/L Fe (as Fe₂(SO₄)₃) using ZnO powder to control the pH in a continuous reactor. p.43

Figure 16. X-ray diffractogram of a poorly crystalline synthetic iron precipitate produce at 60°C and a pH of 2.75 in a continuous crystallizer. p.46

Figure 17. Phase stability of iron precipitates in terms of relative supersaturation and pH. p.47

Figure 18. Filter cake moisture content for iron precipitates produced in a continous crystallizer from a hot iron solution containing 5 g/L H₂SO₄ and 10 g/L Fe (as Fe₂(SO₄)₃) using ZnO powder as neutralising agent as a function of pH and temperature. p.50

Figure 19. Influence of pH and temperature on precipitate solids density for iron precipitates produced in a continous crystallizer from a hot iron solution containing 5 g/L H₂SO₄ and 10 g/L Fe (as Fe₂(SO₄)₃) using ZnO powder as neutralising agent. p.51

Figure 20. Influence of pH and temperature on precipitate mean particle size for iron precipitates produced in a continous crystallizer from a hot iron solution containing 5 g/L H₂SO₄ and 10 g/L Fe (as Fe₂(SO₄)₃) using ZnO powder as neutralising agent. p.52

Figure 21. Influence of pH and temperature on precipitate population density obtained from Malvern particle analyses for iron precipitates produced in a continous crystallizer from a hot iron solution containing 5 g/L H₂SO₄ and 10 g/L Fe (as Fe₂(SO₄)₃) using ZnO powder as neutralising agent. p.52

Figure 22. Influence of pH and temperature on the zinc content of iron precipitates produced in a continous crystallizer from a hot iron solution containing 5 g/L H₂SO₄ and 10 g/L Fe (as Fe₂(SO₄)₃) using ZnO powder as neutralising agent. p.53

Figure 23. Illustration of the difference between mixing times and precipitation (nucleation and growth) rates [Adapted from Vicum *et al.*, 2004]. p.55

Figure 24. Three-zone model used to study the influence of mixing on iron precipitate product quality [Adapted from Gösele and Kind, 1991]. p.57

Figure 25. Dimensions of the draft tube reactor used to precipitate iron from a hot iron solution. p.65

Figure 26. Dimensions of the fluidised bed reactor used to precipitate iron from a hot iron solution. p.65

Figure 27. Effect of iron solution and oxidised slurry recirculation on specific filter resistance for iron precipitated from an iron solution containing 5 g/L H_2SO_4 and 10 g/L Fe added as $Fe_2(SO_4)_3$ using a 5% ZnO slurry as neutralising agent. p.70

Figure 28. Effect of iron solution and oxidised slurry recirculation on specific filter resistance for iron precipitated from an iron solution containing 5 g/L H_2SO_4 and 10 g/L Fe added as $Fe_2(SO_4)_3$ using a 5% ZnO slurry as neutralising agent. p.71

Figure 29. Effect of solution recirculation on the zinc content of iron precipitated from an iron solution containing 5 g/L H_2SO_4 and 10 g/L Fe added as $Fe_2(SO_4)_3$ using a 5% ZnO slurry as neutralising agent. p.72

Figure 30. Effect of solution recirculation on the iron content of iron precipitated from an iron solution containing 5 g/L H_2SO_4 and 10 g/L Fe added as $Fe_2(SO_4)_3$ using a 5% ZnO slurry as neutralising agent. p.72

Figure 31. Effect of mixing time on the specific filter resistance of iron precipitated from an iron solution containing 5 g/L H_2SO_4 and 10 g/L Fe added as $Fe_2(SO_4)_3$ using a 5% ZnO slurry as neutralising agent. p.75

Figure 32. Effect of stirring rate, i.e. micromixing on specific filter resistance of iron precipitated from an iron solution containing 5 g/L H_2SO_4 and 10 g/L Fe added as $Fe_2(SO_4)_3$ using a 5% ZnO slurry as neutralising agent. p.76

Figure 33. SEM image of agglomerated iron particles A (ferrihydrite) and B (schwertmannite) found in an industrial iron residue produced in the Zincor iron removal process. It also appears as though particle B consists of agglomerated primary particles and clusters of primary particles [Claassen, 2002]. p.88

Figure 34. Influence of pH on the degree of agglomeration for the precipitation of metastable iron phases at 60°C and stirring rate of 600 rpm from an iron solution containing 10 g/L Fe added as $\text{Fe}_2(\text{SO}_4)_3$ and 5 g/L H_2SO_4 . A 2.5% ZnO slurry was used as neutralizing agent. p.97

Figure 35. Influence of temperature on the degree of agglomeration for the precipitation of metastable iron phases at a pH of 3.0 and stirring rate of 600 rpm from an iron solution containing 10 g/L Fe added as $\text{Fe}_2(\text{SO}_4)_3$ and 5 g/L H_2SO_4 . A 2.5% ZnO slurry was used as neutralizing agent. p.97

Figure 36. Influence of the initial seed size and seed mass on the degree of agglomeration for the precipitation of metastable iron phases at a pH of 3.2, 65°C and stirring rate of 600 rpm from an iron solution containing 10 g/L Fe added as $\text{Fe}_2(\text{SO}_4)_3$ and 5 g/L H_2SO_4 . A 2.5% ZnO slurry was used as neutralizing agent. p.100

Figure 37. Influence of the initial seed mass on the final mean particle size for the precipitation of metastable iron phases at a pH of 3.2, 65°C and stirring rate of 600 rpm from an iron solution containing 5, 10 and 15 g/L Fe added as $\text{Fe}_2(\text{SO}_4)_3$ and 5 g/L H_2SO_4 . A 2.5% ZnO slurry was used as neutralizing agent. p.101

Figure 38. Influence of the initial seed concentration on precipitate zinc content for metastable iron phases formed at a pH of 3.2, 65°C and stirring rate of 600 rpm from an iron solution containing 10 g/L Fe added as $\text{Fe}_2(\text{SO}_4)_3$ and 5 g/L H_2SO_4 . A 2.5% ZnO slurry was used as neutralizing agent. p.103

Figure 39. Influence of the initial seed concentration on precipitate sulphate content for metastable iron phases formed at a pH of 3.2, 65°C and stirring rate of 600 rpm from an iron solution containing 10 g/L Fe added as $\text{Fe}_2(\text{SO}_4)_3$ and 5 g/L H_2SO_4 . A 2.5% ZnO slurry was used as neutralizing agent. p.104

Figure 40. Influence of the initial seed concentration on the specific filter resistance of metastable iron phases formed at a pH of 3.2, 65°C and stirring rate of 600 rpm from an iron solution containing 10 g/L Fe added as $\text{Fe}_2(\text{SO}_4)_3$ and 5 g/L H_2SO_4 . A 2.5% ZnO slurry was used as neutralizing agent. p.105

Figure A1.1. Nucleation data for ferric iron determined at 50, 70 and 90°C. The pH was changed stepwise in increments of 0.5 pH units every 20 minutes. The pH was increased by adding $\text{Ca}(\text{OH})_2$ and ZnO powder and decreased by adding 98% H_2SO_4 . p116.

Figure A1.2. Solubilization data for ferric iron determined at 50, 70 and 90°C. The pH was changed stepwise in increments of 0.5 pH units every 20 minutes. The pH was increased by adding $\text{Ca}(\text{OH})_2$ and ZnO powder and decreased by adding 98% H_2SO_4 . p116.

Figure A1.3. Particle size distribution of the seed material used to determine the influence of seed mass on agglomeration as determined by a Malvern Mastersizer. p 117.

Figure A2.1. Ferric ion stability diagram determined with the STABCAL™ NBS-database at 50°C. p117.

Figure A2.2. Ferric ion stability diagram determined with the STABCAL™ NBS-database at 70°C. p118.

Figure A2.3. Ferric ion stability diagram determined with the STABCAL™ NBS-database at 90°C. p118.

LIST OF TABLES

Table 1. Iron phases expected to be present in Zincor's iron residue [Claassen *et al.*, 2002]. p.17

Table 2. Summary of ionic and hydrolytic precipitation methods [Habashi, 1999]. p.21

Table 3. Experimental conditions used to determine the influence of stagewise precipitation on product quality. p.33

Table 4. Average hot iron solution (HIS) and ZnO slurry flow rates used to precipitate iron at different pH setpoints. p.35

Table 5. X-ray diffraction results obtained from synthetic iron precipitate samples produced in a continuous reactor at 60°C. p.44

Table 6. Results obtained from stagewise iron removal experiments performed at 65°C. p.48

Table 7. Variables and their ranges used to determine the RTD and mean residence times in a CSTR and DTB reactor. p.59

Table 8. Experimental parameters used to determine the influence of solution exchange rates on iron precipitate product quality using the three-zone model approach. p.61

Table 9. Purity of the calcine used to precipitate iron using the three-zone model approach. p.62

Table 10. Experimental parameters used to determine the influence of solution exchange rates on iron precipitate product quality using the three-zone model approach and industrial zinc calcine as neutralising agent. p.62

Table 11. Experimental parameters used to determine the influence of mixing time on iron precipitate product quality using the three-zone model approach. p.63

Table 12. Experimental parameters used to determine the influence of micromixing on iron precipitate product quality using the three-zone model approach. p.64

Table 13. Experimental parameters used to determine the influence of reactor design on iron precipitate quality. p.66

Table 14. Experimental parameters used to determine the influence of feed point location on iron precipitate quality. p.67

Table 15. The effect of applying the three-zone model approach on iron precipitate quality when industrial zinc calcine was used as neutralising agent. p.74

Table 16. Average specific filter of iron precipitates produced in different continuous reactors. p.78

Table 17. Influence of the type of reactor used for iron precipitation on the quality of the final product. p.80

Table 18. Influence of feed point location on iron precipitate quality. p.81

Table 19. Average mean residence times calculated for different mixing regimes using residence time distribution data. p.82

Table 20. Different nucleation and growth mechanisms encountered in crystallization and precipitation processes [After Dirksen and Ring, 1991]. p.85

Table 21. Parameters and their values used to determine their relative influence on the agglomeration of metastable iron phases. p.91

Table 22. Hadamard matrix of the parameters evaluated. p.91

Table 23. Experimental conditions used to evaluate changes in the initial seed mass on precipitate product quality. p.93

Table 24. Experimental conditions used to evaluate changes in the initial seed size on precipitate product quality. p.93

Table 25. Precipitate characteristics obtained for the operating variables indicated. p.94

Table 26. Relative importance of the different operating parameters evaluated. p.94

Table A3.1. Spreadsheet used to calculate particle population density from Malvern particle analysis data. p119.

REFERENCE LIST

Arregui, V., Gordon, A.R., and Steinveit, G., 1980. The Jarosite Process – Past, Present and Future. Lead-Zinc-Tin '80. Proceedings of the 109th Annual Meeting, Las Vegas, Nevada, February 24-28, 97-123.

Ashurst, K.G. and Hancock, R.D., 1977. The thermodynamics of the formation of sulphate complexes of iron(III), cobalt(II), iron(II), manganese(II) and copper(II) in perchlorate medium. NIM Report No. 1914, Randburg, South Africa.

Babcan, J., 1971. Synthesis of Jarosite - $KFe_3(SO_4)_2(OH)_6$. Geol. Zb., 22 (2), 299-304.

Baldyga, J. and Orciuch, W., 2001. Some hydrodynamic aspects of precipitation. Powder Technology, 121, 9-19.

Bigham, J. M., Carlson, L. and Murad, E., 1994. Schwertmannite, a new iron oxyhydroxy-sulphate from Pyhasalmi, Finland, and other localities. Min. Mag., 58, 641-648.

Bigham, J.M., Schwertmann, U., Carlson, L. and Murad, E., 1990. A poorly crystallized oxyhydroxysulfate of iron formed by bacterial oxidation of Fe(II) in acid mine waters. Geochim. Cosmochim. Acta, 54, 2743 – 2758.

Bigham, J.M., Schwertmann, U., Traina, S.J., Winland, R.L. and Wolf, M., 1996. Schwertmannite and the chemical modeling of iron in acid surface waters. Geochim. Cosmochim. Acta, 60, 2111 – 2121.

Claassen, J.O., 2002. Characterization and optimization of the Zincor iron removal process. M. Eng. Thesis. University of Pretoria, Pretoria, South Africa, 149p.

Claassen, J.O., Meyer, E.H.O., Rennie, J. and Sandenbergh, R.F., 2002. Iron removal from zinc-rich process solutions: Defining the Zincor Process. Hydrometallurgy, 67, 87-108.

Claassen, J.O., Meyer, E.H.O., Rennie, J. and Sandenbergh, R.F., 2003(a). Iron precipitation from zinc-rich process solutions: Optimizing the Zincor Process, J. SAIMM, May 2003, 253 - 263.

Claassen, J.O., Rennie, J., Van Niekerk W.H., Meyer, E.H.O. and Sandenbergh, R.F., 2003(b). Recent developments in iron removal and control at the Zinc Corporation of South Africa. Hydrometallurgy 2003, 5th International Symposium Proceedings. C. Young, A. Alfantazi, C. Anderson, A. James, D. Dreisinger, B. Harris, (Eds.). TMS, Canada, 1675 – 1690.

Chen, T.T. and Cabri, L.J., 1986. Mineralogical overview of iron control in hydrometallurgical processing. Proceedings of the First International Symposium on Iron Control in Hydrometallurgy, J.E. Dutrizac and A.J. Monhemius, (Eds.), Ellis Horwood, England, 19 – 55.

Cornell, R.M. and Schwertmann, U., 1996. The Iron Oxides - Structure, Properties, Reactions, Occurrence and Uses. Weinheim, New York, 573p.

Cubeddu, F., Piasentin, M. and Reilly, F., 1996. The para-goethite process at the Enirisorse-Porto Vesme plant. Proceedings of the Second International Symposium on Iron Control in Hydrometallurgy, J.E. Dutrizac and G.B. Harris, (Eds.), The Canadian Institute of Mining, Metallurgy and Petroleum, Ottawa, Canada, 147 – 162.

David, R. and Klein, J., 2001. Reaction Crystallization. Crystallization Technology Handbook, Mersmann, A. (Ed.), New York, Marcel Dekker Inc., 832p.

Demopoulos, G., 1993. Precipitation in aqueous processing of inorganic materials: A unified colloid-crystallization approach to the production of powders with controlled properties. First International Conference on Processing Materials for Properties, H. Henein and T. Oki, (Eds.), The Minerals, Metals and Materials Society, 537 – 540.

Demopoulos, G. P., 2003. Short Course: Aqueous precipitation and crystallization for the production of particulate solids with desired properties. Hydrometallurgy 2003, 5th International Symposium Proceedings, Vancouver, Canada.

Dirksen, J. A. and Ring, T. A., 1991. Fundamentals of crystallization: kinetic effects on particle size distribution and morphology. *Chem. Eng. Sci.*, 46 (10), 2389-2427.

Dutrizac, J.E., 1985. Jarosite type compounds and their application in the metallurgical industry. *Hydrometallurgy, Research, Developments and Plant Practice. Proc. 112th AIME Annual Meeting*, K. Osseo-Asare and J.D. Miller, (Eds.), TMS-AIME, Atlanta, Georgia, 6-10 March 1985, 531 – 551.

Dutrizac, J.E., 1999. Determination of schwertmannite in hydrometallurgical leach residues. Part 1 – The Nature of Schwertmannite. Part 2 – Examination of Hydrometallurgical Leach Residues, Department of Public Works and Government Services Canada, Contract 028SQ.23440-7-1012, unpublished.

Fogler, H.S., 1999. *Elements of Chemical Reaction Engineering*, 3rd Edition, N.R. Amundson, (Ed.), Prentice Hall, New Jersey, 967p.

Franke, J. and Mersmann, A., 1995. The influence of the operational conditions on the precipitation process. *Chem Eng. Sci.*, 50 (11), 1737-1753.

Garside, J., Gaska, J. and Mullin, J. W., 1972. *J. Crystal Growth*, 13/14, 510.

Garside, J., 1977. Kinetics of crystallization from solutions. *Crystal growth and Materials*, Kaldis, E. and Scheel, H. J. (Eds.), North-Holland, Amsterdam, 484p.

Gordon, A.R. and Pickering, R.W., 1975. Improved leaching technologies in the electrolytic zinc industry. *Metal. Trans.*, 6B, 43-53.

Gösele, W., Egel-Hess, W., Wintermantel, K., Faulhaber, F. R. and Mersmann, A., 1990. Feststoffbildung durch Fällung. *Chem. Inge. Tech.*, 62, 544-552.

Gösele, W. and Kind, M., 1991. Study on the influence of mixing on the quality of continuous precipitating products. *Chem. Ing. Tech.*, 63, 59 - 62.

Habashi, F., 1999. Textbook of Hydrometallurgy. Metallurgie Extractive, Quebec, Canada, 739p.

Ilievski, D. and White, E.T., 1994. Agglomeration mechanisms in $\text{Al}(\text{OH})_3$ crystallization from caustic aluminate solutions. Proceedings of the First International Technology Forum, Denver, Co, AIChE, New York, 305 – 310.

Jambor, J.L. and Dutrizac, J. E., 1998. Occurrence and constitution of natural and synthetic ferrihydrite, a widespread iron oxy-hydroxide. Chemical Reviews, 98 (7), 2549 – 2585.

Johnston, J.R.R. and Cresswell, P.J., 1996. Modelling alumina precipitation: dynamic solution of the population balance equation. Fourth International Alumina Quality Workshop, Darwin, June 1996, 281 – 290.

Kind, M., 2002. Colloidal aspects of precipitation processes. Chem. Eng. Sci., 57, 4287-4293.

Loan, M., Parkinson, G., Newman, M. and Farrow, J., 2001. Iron oxy-hydroxide crystallization in a hydrometallurgical residue. J. of Crystal Growth, 235, 482-488.

McCristal, T.G. and Manning, J., 1998. Conversion of the Pasminco Hobart Smelter to para-goethite. Zinc and Lead Processing. J. E. Dutrizac, J. A. Gonzales, G.L. Bolton and P. Hancock, (Eds.), The Metallurgical Society of CIM, 439 – 453.

Mersmann, A., 2001. Fundamentals of crystallization. Crystallization technology handbook, 2nd Edition, Mersmann, A. (Ed.), New York, Marcel Dekker, 832p.

Meyer, E.H.O., Howard, G., Heagele, R. and Beck, R.D., 1996. Iron control and removal at the Zinc Corporation of South Africa. Proceedings of the Second International Symposium on Iron Control in Hydrometallurgy, J.E. Dutrizac and G.B. Harris, (Eds.), The Canadian Institute of Mining, Metallurgy and Petroleum. Ottawa, Canada, 163 – 182.

Mullin, J. W., (Ed.), 1972. Crystallization, 2nd Edition, Butterworths, London, 480p.

Mullin, J. W., (Ed.), 1976. Industrial Crystallization, Plenum Press, New York.

Mullin, J. W. and Ang, N. M. 1976. Disc. Faraday Soc., 61, 141.

Nielsen, A.E., (Ed.), 1964. Kinetics of precipitation, Pergamon Press, New York.

Nielsen, A.E., 1967. Crystal Growth, Peiser H.S. (Ed.), Pergamon Press, New York, 419p.

Nyvt, J., (Ed.), 1971. Industrial crystallization from solutions, Butterworths, London.

Nyvt, J., (Ed.), 1982. Industrial Crystallization: the state of the art. 2nd Edition, Verlag Chemie, Weinheim, 182p.

Nyvt, J., Söhnel, O., Matuchova, M. and Broul, M., 1985. The Kinetics of Industrial Crystallization, Chemical Engineering Monograph Series, 19, Elsevier, Amsterdam, 350p.

Onozaki, A., Sato, K. and Kuramochi, S., 1986. Effect of some impurities on iron precipitation at the Iijima Zinc Refinery. Proceedings of the First International Symposium on Iron Control in Hydrometallurgy, J.E. Dutrizac and A.J. Monhemius, (Eds.), Ellis Horwood, England, 742 - 752.

Pammenter, R.V., Kershaw, M.G. and Horsham, T.R., 1986. The Low-contaminant Jarosite Process – Further developments and the implementation of the process. Proceedings of the First International Symposium on Iron Control in Hydrometallurgy, J.E. Dutrizac and A.J. Monhemius, (Eds.), Ellis Horwood, England, 603 - 617.

Pamplin, B.R., (Ed.), 1975. Crystal Growth. International series of monographs in the science of the solid state, Volume 6, 672p.

Patent, 1964, Asturiana de Zinc S. A., Spanish Patent No. 304,601, Application lodged October 1964. Equivalent U.S. Patent No. 3,434,798 granted March 25, 1969.

Patent, 1965(a), Det Norske Zinkkompani A/S Norwegian Patent NO. 108,047, Application lodged April 30, 1965. Equivalent U.S. Patent No. 3,434,947 granted March 25, 1969.

Patent, 1965(b), Electrolytic Zinc Company of Australasia Limited, Australian Patent No. 401,724. Application lodged 31st March, 1965. Equivalent U.S. Patent No. 3,493,365 granted 3rd February, 1970.

Patent, 1966, "Procédé de préparation d'oxydes de fer hydraté", Belgian Patent, No. 676.970,24, February 1966.

Patent, 1972, Societe de la Vieille Montagne, Belgian Patent No. 724,214. Application lodged November 20, 1968, Equivalent U.S. Patent No. 3,652,264, granted March 28, 1972.

Patrizi, A., Persia, G. and Pescetelli, A., 1985. The new electrolytic zinc plant at Porto Vesme, Italy. Zinc '85: International Symposium on Extractive Metallurgy of Zinc, K. Tozawa, (Ed.), The Mining and Metallurgical Institute of Japan. Tokyo, 413 – 434.

Raghavarao, D., 1971. Constructions and Combinatorial Problems in Design of Experiments, Wiley, New York, 274p.

Rosmalen Van, G. M. and Kramer, H. J. M., 1998. Crystallization and Precipitation. Workshop held in Gauteng, South Africa in cooperation with the University of Cape Town, 10-12 June 1998.

Saffman, P.G. and Turner, J.S., 1956. On the collision of drops in turbulent clouds. J. Fluid. Mech., 1, 16.

Sakamoto, K., Kanahara, M. and Matsushita, K., 1976. Agglomeration of crystalline particles of gibbsite during the precipitation in sodium aluminate solutions. *Light Metals*, 2, 149 – 162.

Söhnel, O. and Garside, J., 1992. *Precipitation*, Butterworths, London.

Seyssiecq, I., Veessler, S., Boistelle, R. and Lamerant, J.M., 1998. Agglomeration of gibbsite $\text{Al}(\text{OH})_3$ crystals in Bayer liquors. Influence of the process parameters. *Chem. Eng. Sci.*, 53 (12), 2177-2185.

Tainton, U.C. and Leyson, L.T., 1924. Electrolytic zinc from complex ores. *Trans. AIME*, (LXX), 486 – 522.

Tsunoda, S., Maeshiro, I., Ewi, M. and Sekine, K., 1973. The construction and operation of the Iijima Electrolytic Zinc Plant. *AIME T.M.S. Paper No. A73 – 65*, Chicago.

Uusipaavalniemi, E., and Karlman, S.G., 1996. Handling of iron at the zinc plant in Kokkola. *Proceedings of the Second International Symposium on Iron Control in Hydrometallurgy*, J.E. Dutrizac and G.B. Harris, (Eds.). The Canadian Institute of Mining, Metallurgy and Petroleum, Ottawa, Canada, 101 – 115.

Van Leeuwen, M.L.J., Bruinsma, O.S.L. and Van Rosmalen, G.M., 1996(a). Influence of mixing on the product quality in precipitation. *Chem. Eng. Sc.*, 51 (11), 2595 - 2600.

Van Leeuwen, M.L.J., Bruinsma, O.S.L. and Van Rosmalen, G.M., 1996(b). Three-zone approach for precipitation of barium sulphate. *J. of Crystal Growth*, 166, 1004 - 1008.

Veessler, S., Roure, S. and Boistelle, R., 1994. General concept of hydrargillite $\text{Al}(\text{OH})_3$ agglomeration. *J. of Crystal Growth*, 135, 505 – 512.

Vicum, L., Mazzotti, M. and Baldyga, J., 2004. Modelling of stirred tank mixing-precipitation processes. Proceedings of the Swiss Symposium on Crystallization and Precipitation, Switzerland, March 2004.

Walton, A.G., 1967. The formation and properties of precipitates. Monographs on Analytical Chemistry and its Applications, Volume 23. Elving P.J. and Kolthoff, I.M. (Eds.), Interscience, New York, 232p.

Walton, A.G., 1969. Nucleation. Zettlemoyer A. C. (Ed.). New York, Marcel Dekker Inc., 225p.

Yakovlev, Y.B., Kul'ba, F.Y., Pus'ko, A.G. and Gerchikova, M.N., 1977. Hydrolysis of iron(III) sulphate in zinc sulphate solutions at 25, 50 and 80°C. Russ. J. Inorg. Chem., 22 (1), 27 – 29.

Yamada, K., 1980. Nucleation and aggregation during crystallization of aluminium tri-oxide in sodium aluminate solution. J. Japanese Inst. Light Metals, 32 (12), 720-726.